


Article

Research on Rapid Detection for TOC in Water Based on UV-VIS Spectroscopy and 1D-SE-Inception Networks

Yu Li ¹, Weihong Bi ^{1,*}, Yajie Jia ¹, Bing Wang ², Wa Jin ¹, Guangwei Fu ¹ and Xinghu Fu ¹ 

¹ School of Information Science and Engineering, The Key Laboratory for Special Fiber and Fiber Sensor of Hebei Province, Yanshan University, Qinhuangdao 066004, China; li_yu@stumail.ysu.edu.cn (Y.L.); jiayajie0811@stumail.ysu.edu.cn (Y.J.); jinwa@ysu.edu.cn (W.J.); earl@ysu.edu.cn (G.F.); fuxinghu@ysu.edu.cn (X.F.)

² Qinhuangdao Hongyan Photoelectric Technology Co., Ltd., Qinhuangdao 066100, China; wangbing@qhdhygd.com

* Correspondence: bwhong@ysu.edu.cn; Tel.: +86-335-8057124

Abstract: In recent years, the rapid monitoring of total organic carbon (TOC) in natural waters has attracted increasing attention. Optical methods are a valid tool for measurement. Nevertheless, how to more accurately establish the mapping relationship between spectroscopy and TOC concentrations is currently a challenge. A new method based on UV-VIS spectroscopy with a deep convolutional network is proposed for the quantification of TOC in water in this paper. The Inception network, originally used to process two-dimensional image data, was redesigned as a model capable of processing one-dimensional spectral data, while the convolution and pooling scale were modified to adapt to one-dimensional data. Simultaneously, squeeze and extraction (SE) blocks were applied to the designed network to enhance feature information and to suppress interference from useless information in the regression process. The method was tested on samples collected from the sea and river estuaries in several provinces in China. When compared to the classical least squares support vector machine (LSSVM), the experimental results showed that the proposed 1D-Inception network structure can provide more accurate regression results. The SE block can significantly improve the feature extraction and expression capabilities of the 1D-Inception network structure and suppress redundant information, thereby achieving better model performance.

Keywords: total organic carbon; UV-VIS absorption spectrum; quick detection; 1D-SE-Inception



Citation: Li, Y.; Bi, W.; Jia, Y.; Wang, B.; Jin, W.; Fu, G.; Fu, X. Research on Rapid Detection for TOC in Water Based on UV-VIS Spectroscopy and 1D-SE-Inception Networks. *Water* **2023**, *15*, 2537. <https://doi.org/10.3390/w15142537>

Academic Editor: Marisa Almeida

Received: 6 June 2023

Revised: 30 June 2023

Accepted: 6 July 2023

Published: 11 July 2023



Copyright: © 2023 by the authors. Licensee MDPI, Basel, Switzerland. This article is an open access article distributed under the terms and conditions of the Creative Commons Attribution (CC BY) license (<https://creativecommons.org/licenses/by/4.0/>).

1. Introduction

In recent years, with the gradual progress of China's industrialisation and agricultural modernisation, and the continuous improvement of its economic status, a large amount of wastewater and agricultural or domestic sewage has been discharged into oceans or rivers, leading to increasingly serious water pollution [1–5]. The deterioration of a water resource poses a serious threat to human life and health. The degree of organic matter pollution of a water body can generally be expressed in terms of its total organic carbon (TOC) or dissolved organic carbon (DOC). Meanwhile, organic carbon in water is an important component of the biogeochemical system and also a key indicator for marine carbon cycle and climate research [6–9].

The general method for analysing TOC or DOC in water is generally by high temperature catalytic oxidation (HTCO) or wet chemical oxidation (WCO) [10–12], which is often utilized in modern TOC analyzers. In the above two methods, all carbon in the water is oxidized to carbon dioxide and the total organic carbon is then determined by measuring the weight of the carbon dioxide using a series of specialized instruments to remove interference from inorganic carbon and collect the carbon dioxide. While these standard methods are accurate, they have drawbacks in practical applications, such as long consumption times, expensive equipment and susceptibility to secondary contamination. Thus, ion

chromatography [13], HPLC-SEC [14], spectrometry [15,16], etc., have emerged as new rapid detection methods for organic carbon in recent years. Due to the advantages of rapid detection and simple instrumentation, and the fact that it requires no additional chemical reagents, the spectroscopic method is currently a relatively inexpensive and widely used measurement method. This method analyzes and measures information by establishing the mapping relationship between organic carbon and spectral parameters [17,18].

Kim and Ji [19] proposed an optical system which uses UV LEDs (280 nm) and photodetectors to determine the content of organic compounds in water. Causse et al. [20] used a combination of second order derivatives at 226 and 295 nm for DOC and nitrate measurements in small rivers in agricultural watersheds, correcting for the effect of nitrate on the long-range UV absorption spectra. Carter et al. [21] accurately predicted dissolved organic carbon from absorbance at 270 nm and 350 nm. Peacock et al. [22] found a strong correlation between DOC and absorbance at wavelengths of 230 and 263 nm. Wang et al. [23] showed a very high regression correlation between the area below 250–350 nm spectra and the concentrations of natural organic matter (NOM) in water. Avagyan et al. [24] added 600 and 740 nm in combination with the traditional 254–400 nm wavelengths using PLS and multiple stepwise regression (MSR) to improve the accuracy of DOC measurements.

In addition to some wavelength combination methods, some scholars use the full spectrum to predict organic content through chemometric methods. Dahlen et al. [25] used first order derivative spectroscopy in the 200–300 nm range and a PLS algorithm to obtain a detection model for non-purgeable organic carbon (NPOC). Liu and Wang [26] used PLS regression analysis to establish a model relationship between the UV-VIS spectrum and TOC, COD of seawater samples along the coast of Tianjin Bohai Bay. Lourenço et al. [27] used a PLS algorithm to build a UV-VIS spectral TOC detection model for water samples (high concentration) collected at the outlet of a wastewater treatment plant. Zhang et al. [28] predicted TOC and TSS in a river confluence near Sheffield-on-Loddon based on UV-VIS spectrometry and artificial neural networks (ANN). Table 1 shows the modelling methods and a performance comparison of the above studies.

Table 1. Previous studies on organic matter concentration and UV-VIS.

Reference	Wavelengths	Research Object	Algorithm	Parameters	Optimal Performance
Chihoon Kim [19]	280 nm	potassium hydrogen phthalate solution		TOC	$R^2 = 0.996$
Jean Causse [20]	226 nm; 295 nm	Watersheds in Brittany, France		DOC	$R^2 = 0.961$ RMSEP = 0.953
Heather T. Carter [21]	270 nm; 350 nm	streams and rivers in UK		DOC	DOCpred/DOC = 1.03 rmsd = 1.37;
		stream and lake in Colorado			DOCpred/DOC = 0.99 rmsd = 0.98;
		stream and lake sites in Canada			DOCpred/DOC = 1.11 rmsd = 0.25
Mike Peacock [22]	263 nm	Ditch water		DOC	$R^2 = 0.98$ RMSEP = 1.78
	230 nm	Pore water			$R^2 = 0.93$ RMSEP = 4.79
		Stream water			$R^2 = 0.96$ RMSEP = 1.36

Table 1. Cont.

Reference	Wavelengths	Research Object	Algorithm	Parameters	Optimal Performance
Gen-Shuh Wang [23]	250–350 nm area under the spectra	Nitrohumic acids		NOM	
		Aldrich humic acids			
		Nacalai Tesque humic acids			
Armine Avagyan [24]	250–740 nm 257.5 nm; 380 nm; 730 nm; 292.5 nm	water from Ust-Pojeg mire complex in the Komi Republic	PLS	DOC	$R^2 = 0.981$ RMSE = 2.80
			MSR		$R^2 = 0.986$ RMSE = 2.43
Johan Dahlén [25]	200–300 nm	Wells in the county of Ostergotland, Sweden	PLS	NPOC	$R^2 = 0.962$ RMSEP = 0.51
Xianhua Liu [26]	190–380 nm	Water from Tianjin Bohai Bay, China	PLS	TOC	$R^2 = 0.975$ RMSEP = 3.97
N. D. Lourenço [27]	246–380 nm	Fuel park wastewater treatment plant	PLS	TOC	$R^2 = 0.98$ RMSECV = 4.4
Hongming Zhang [28]	200–800 nm	River confluence near Sherfield-on-Loddon	ANN	TOC	$R^2 = 0.953$ RMSE = 0.395

However, there are few high-accuracy and rapid quantitative studies of TOC directly targeting natural and complex water bodies in multiple regions in the above-related explorations. Therefore, in this paper, a TOC quantification model based on UV-VIS spectroscopy and a deep convolutional network is proposed. This detection model was trained on ocean and river estuary water sampled in several provinces. The model performance of the TOC concentration quantification was evaluated on the test dataset.

2. Materials and Methods

2.1. SE-Inception Network

2.1.1. Inception Principle

Convolutional neural networks (CNN) is a popular algorithm in the field of artificial intelligence and has achieved excellent results in the field of computer vision, starting from LeNet [29] in 1998, until AlexNet [30] renewed attention was paid to the algorithm in 2012. As the computability of computers improved, VGG [31], ResNet [32] and others network structure have emerged, and CNN is becoming deeper and more complex, with its performance improving at the same time.

A typical convolutional network structure is depicted in Figure 1. The initial input tensor passes through a convolutional layer, pooling layer, and flatten layer, respectively, to obtain the desired output results.

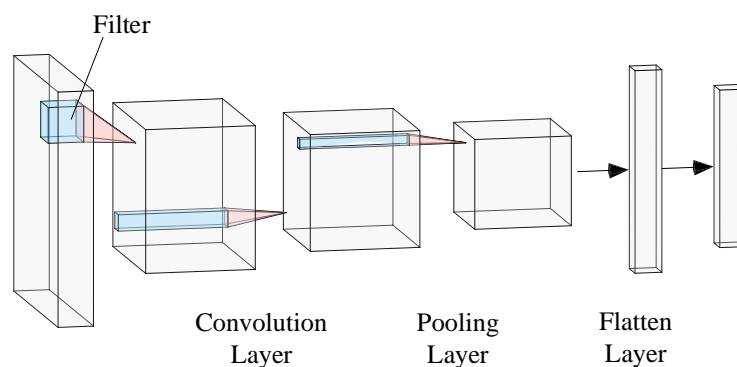


Figure 1. Typical convolutional network structure.

Inception [33] is also a deep learning network based on CNN networks and it solves the problem of excessive stacking parameters in multiple convolutional layers, transforming the network from deeper to wider. The Inception network designs a network with an excellent local topological structure, which performs multiple convolution or pooling operations on the input tensor in parallel and concatenates all output results into a very broad feature map. Inception networks typically consist of several Inception modules connected in series. Figure 2 illustrates the structure of the classical Inception module, which passes the input tensors through the layer that 1×1 convolution, 1×1 and 3×3 convolutions, 1×1 and 3×3 convolutions, pooling layer and 1×1 convolution, and concatenates the above calculation results into the output.

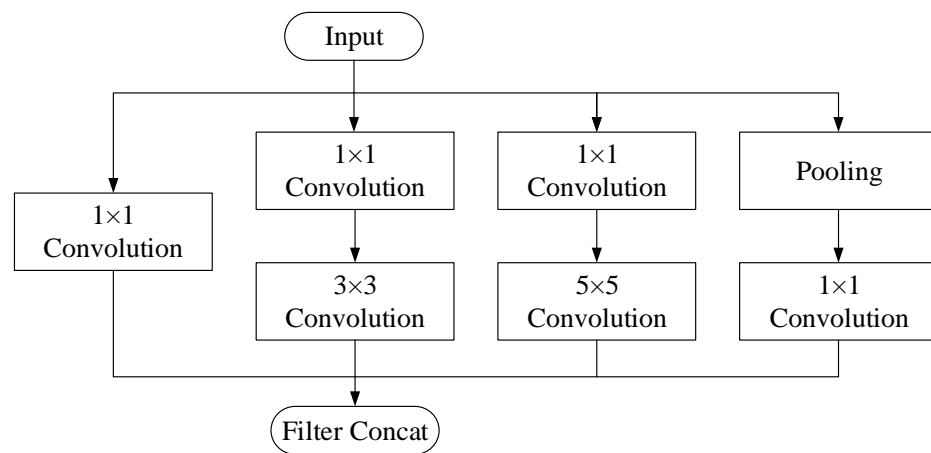


Figure 2. Inception module structure.

2.1.2. SE Module

The structure of the SE (squeeze and excitation) module [34] is shown in Figure 3. The SE blocks can be thought of as an attention function that is used for any given transformation F_{tr} . In deep learning, F_{tr} is usually a convolutional operator. Input tensor $X \in \mathbb{R}^{H' \times W' \times C'}$ is transformed to $U \in \mathbb{R}^{H \times W \times C}$ by F_{tr} .

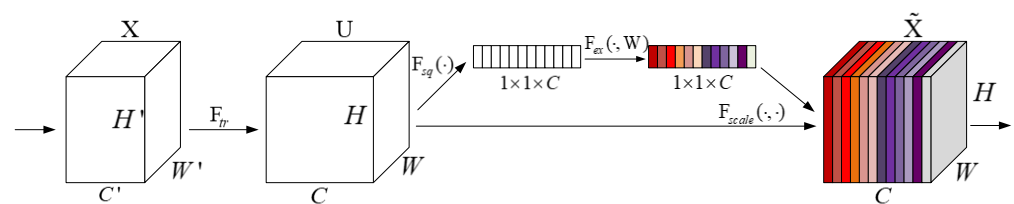


Figure 3. Squeeze and Excitation block.

First, the global spatial information of the tensor U is squeezed into the channel descriptor so that it to be utilized by other input layers. The statistic $z \in \mathbb{R}^C$ is calculated by:

$$z_c = F_{sq}(u_c) = \frac{1}{H \times W} \sum_{i=1}^H \sum_{j=1}^W u_c(i, j) \tag{1}$$

Subsequently, each channel learns a function of specific samples which enables the use of global information, effectively emphasizing information features and suppressing less useful features through a channel-dependent self-selection gate mechanism with a sigmoid activation. ReLU activation is applied to limit complexity:

$$s = F_{ex}(z, W) = \sigma(g(z, W)) = \sigma(W_2 \text{ReLU}(W_1 z)), \tag{2}$$

where $W_1 \in \mathbb{R}^{\frac{C}{r} \times C}$ and $W_2 \in \mathbb{R}^{C \times \frac{C}{r}}$, ratio r choss 16 in this article to effectively balance accuracy and complexity.

Finally, the result is obtained by weighting the previous weight to the input features channel by channel through multiplication:

$$\tilde{x}_c = F_{scale}(u_c, s_c) = s_c \cdot u_c \tag{3}$$

where $\tilde{X} = [\tilde{x}_1, \tilde{x}_2, \dots, \tilde{x}_c]$ and $F_{scale}(u_c, s_c)$ represents the result of channel-weighting multiplication between the scale s_c and the feature tensor $u_c \in \mathbb{R}^{H \times W}$. Different colors in the tensor \tilde{X} in Figure 3 represent different weights assigned in the channel.

2.1.3. 1D-SE-Inception Block

Due to the fact that the UV-VIS absorption spectra collected in this article are 1D data, and the original Inception network input is 2D image data, the convolutional kernel in this article was accordingly changed from a 2D structure to a 1D structure, i.e., the convolutional kernel $1 \times 1, 3 \times 3$ was transformed to $1 \times 1, 1 \times 3$. The 1D-InceptionV1 network converted a 5×5 convolutional kernel into a 1×5 convolutional kernel. The 1D-Inception V2 network converted a 1×5 convolutional kernel into double 1×3 convolutional kernels to improve network performance and reduce computational complexity. The 1D-Inception was added to an SE module which was the specific structure of connecting two fully connected layers after the global pooling layer. The size of the first FC layer was $1 \times 1 \times \frac{C}{r}$ with the ReLU activation function, the size of second FC layer was $1 \times 1 \times C$ with the sigmoid activation function. The 1D-SE-Inception block is depicted in Figure 4.

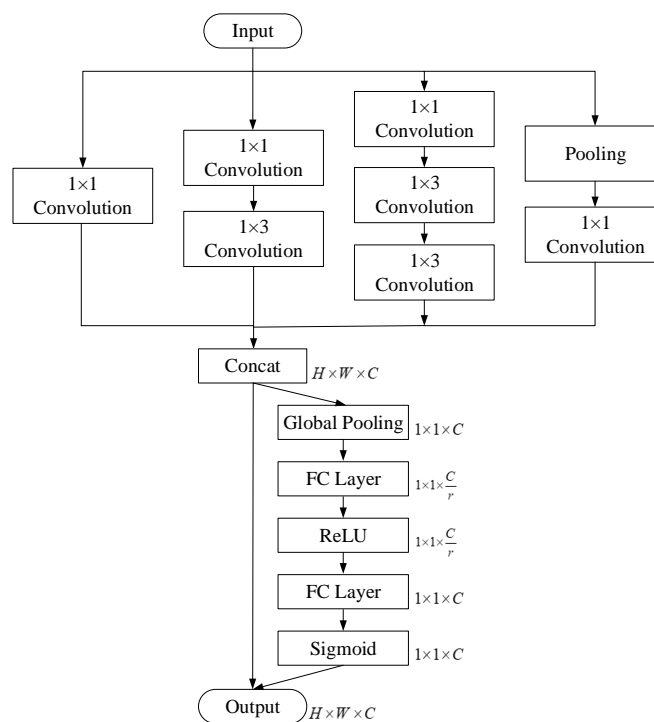


Figure 4. 1D-SE-Inception block.

2.1.4. 1D-SE-Inception Network Structure

The 1D-SE-Inception network structure used in this experiment is shown in Figure 5. The first part of Figure 5 shows the initial input block of the network. First, the overall features of the input spectra were extracted by 1×7 convolutional layers, then the size was reduced by max-pooling layers. Second, the detailed features of the input spectra

were extracted by 1×3 and 1×3 convolutional layers, then the size was reduced by max-pooling layers.

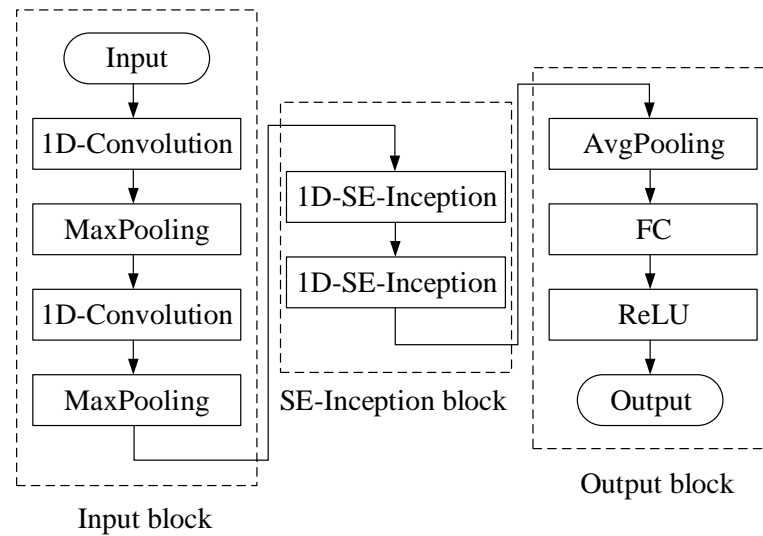


Figure 5. 1D-SE-Inception network structure.

The second part consists of two 1D-SE-Inception blocks. SE blocks are added to the Inception block to assign weights to different information and suppress redundant information, thus improving the model’s ability to extract spectral features. The superposition of two 1D-SE-Inceptions increased the depth of the network, allowing it to fully extract network features and achieve a balance between accuracy and complexity.

The third part is the output block. The features extracted from the 1D-SE-Inception network pass through the average pooling layer, the full connection layer, and then the ReLU activation function calculates the TOC concentration.

2.2. LSSVM Model

The least squares support vector machine (LSSVM) is an extension of SVM that uses the least squares system as a loss function to replace the quadratic programming problem of the traditional SVM, transforming the problem into one of solving a set of equations.

If the sample from the water spectrum data is $\{x_i, y_i\}$, its regression function $f(x)$ is expressed as:

$$f(x) = w^T \varphi(x) + b \tag{4}$$

where w^T is the weight vector, $\varphi(x)$ is the mapping function from input information space to high-dimensional space, and the b is the offset.

The optimization problem for regression correspondence is

$$\min_{w,b,e} Q(w, b, e) = \frac{1}{2} \|w\|^2 + \frac{\gamma}{2} \sum_{i=1}^l e_i^2 \tag{5}$$

$$s.t. y_i = w^T \varphi(x_i) + b + e_i \quad (i = 1, 2, \dots, l) \tag{6}$$

where e_i is error variable of the i th data, γ is the penalty parameters for error adjustment.

The corresponding Lagrange function is

$$L(w, b, e, a) = Q(w, b, e) - \sum_{i=1}^l \alpha_i [w^T \varphi(x_i) + b + e_i - y_i] \tag{7}$$

According to the KKT and Mercer conditions, the regression function is

$$y(x) = \sum_{i=1}^l \alpha_i K(x, x_i) + b \tag{8}$$

where $\alpha = A^{-1} \begin{pmatrix} y - b \mathbf{1} \\ \mathbf{1} \end{pmatrix}$, $b = \frac{\mathbf{1}^T A^{-1} y}{\mathbf{1}^T A^{-1} \mathbf{1}}$, $A = \Omega + \gamma^{-1} I$, $\Omega_{ij} = K(x_i, y_j) = \varphi^T(x_i) \varphi(y_j)$.

This paper adopted an RBF kernel function:

$$K(x, x_i) = e^{-\frac{\|x-x_i\|^2}{2\sigma^2}}, (\sigma > 0) \tag{9}$$

2.3. Experiment

2.3.1. Water Sampling

Water samples for this investigation were collected over four seasons from 2019 to 2023 from the marine areas, river estuaries and lakes in Qinhuangdao, Hebei Province, Weihai, Shandong Province, Tianjin, etc. Water samples were collected in 500 mL brown reagent bottles and always stored in a refrigerator at 4 °C prior to testing in order to restrain and slow down the oxidative consumption of organic matter by microorganisms.

2.3.2. TOC Measurements

The concentration of total organic carbon was analyzed by TOC-L CPH (Shimadzu, Japan), which used the 720 °C combustion catalytic oxidation method and the non-dispersive infrared absorption method to measure carbon dioxide. There were 390 water samples with a TOC ranging from 1.470–18.37 mg/L.

2.3.3. UV-VIS Absorption Spectroscopy Measurement

The water sample was restored to room temperature prior to UV-VIS spectral measurement. The UV-VIS absorption spectroscopy measurements of water samples were performed using AvaSpec-2048 Ultraviolet Visible Fiber Spectrometer (Avantes, Apeldoorn, The Netherlands), AvaLight-DH-S-BAL Deuterium/Halogen Combined Fiber Optic Source and a quartz cell with 10 mm path length. The integration time was set to 2 ms with an average of 200 sampling times and the wavelength ranged from 200 nm to 600 nm. Water sample spectra were collected three times and the average of the spectra was taken.

All calculations were carried out on a personal computer equipped with a Windows 10 operating system. The deep convolutional network model used the PyCharm IDE (version 2020.1), Python 3.7 and the Tensorflow 2.0 framework.

2.4. Assessing the Performance of the Model

Generally, Pearson *r* and RMSE are generally used to evaluate model performance. The Pearson *r* statistic ranges from −1 to 1 and the closer to 1 the value of R, the better the detection performance of the model. The closer the RMSE is to 0, the better the model’s ability to detect the following

$$r = \frac{\sum (TOC_{real} - \overline{TOC_{real}}) (TOC_{pre} - \overline{TOC_{pre}})}{\sqrt{\sum (TOC_{real} - \overline{TOC_{real}})^2} \sqrt{\sum (TOC_{pre} - \overline{TOC_{pre}})^2}} \tag{10}$$

$$RMSE = \sqrt{\frac{1}{n} \sum_{i=1}^n (TOC_{pre} - TOC_{real})^2} \tag{11}$$

in which TOC_{real} is the real concentration of TOC and in which TOC_{pre} is the predicted concentration of TOC.

3. Results

3.1. UV-VIS Absorption Spectra of Real Water Samples

The UV-VIS absorption spectra of 390 samples with different TOC concentrations in different regions from 2019 to 2023 were measured experimentally. Due to limited space, only some spectra of the samples were plotted, as shown in Figure 6.

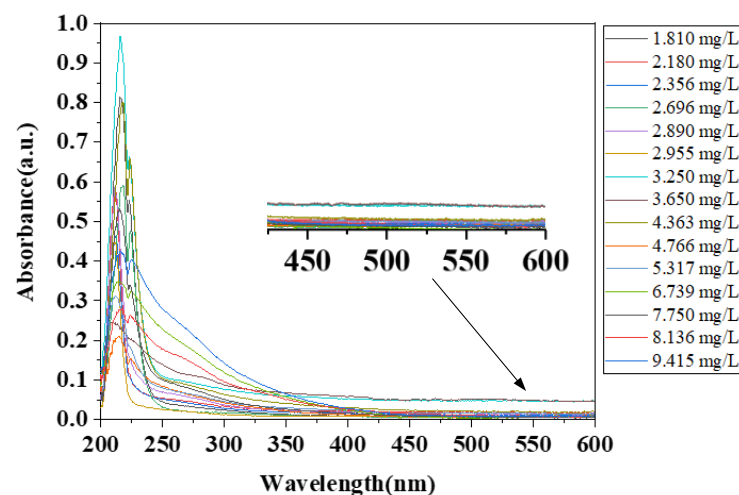


Figure 6. UV-VIS absorption spectra of a selection of water samples.

As shown in Figure 6, the absorption of UV-VIS light by substances in the water is mainly concentrated in the 200–450 nm range, while the spectral absorbance in the 450–600 nm range remains essentially unchanged. Although there is a strong absorption peak near 220 nm, this may be due to the absorption of inorganic compounds such as nitrate or the absorption of humus ubiquitously found in the water. It is impossible to distinguish the substances and contents corresponding to this absorption peak, so it is retained. In the subsequent process, the data-driven mode was selected, that is, the subsequent computation of the neural network was used for feature extraction or suppression. The absorbance of 450–600 nm was mainly due to the undifferentiated scattering of light by turbidity caused by insoluble substances, which contained noise information and less information. For these reasons, a wavelength range of 200–450 nm was chosen for the subsequent modelling.

3.2. Deep Convolutional Network Approach

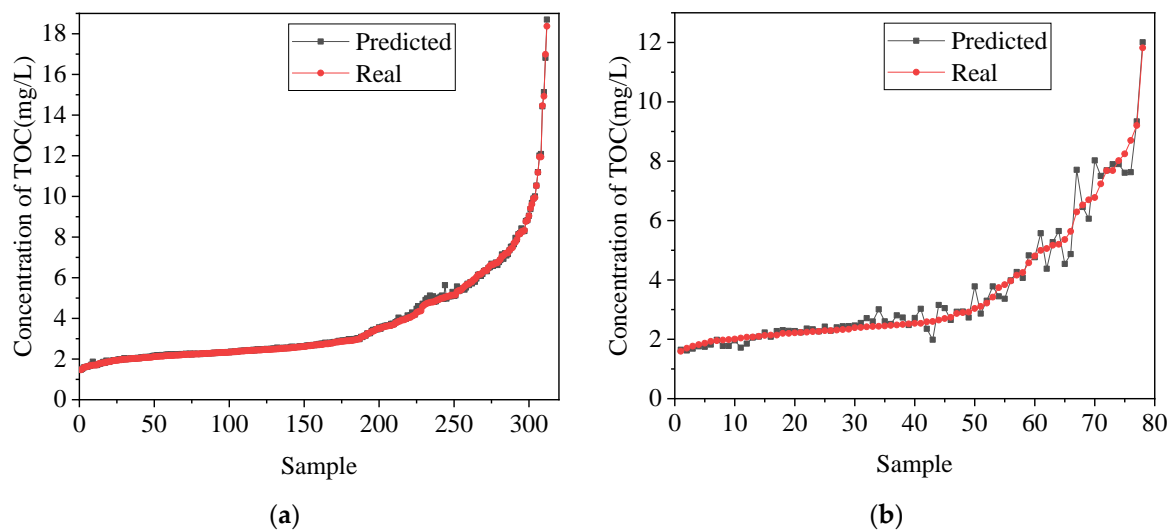
To illustrate the performance of these TOC concentration detection model, 390 samples were collected. According to a ratio of 8:2 between the training set and the test set, 312 samples were randomly selected as the training set and the remaining 78 samples were used as the test set. The TOC concentrations of the training set ranged from 1.470 to 18.37 mg/L, while the testing set ranged from 1.597 to 11.82 mg/L. On each of these training sets, 1D-Inception V1, 1D-Inception V2, 1D-SE-Inception V1, 1D-SE-Inception V2 approaches were fitted to the data and computed the resulting root mean square error on a test set. Quantitative TOC detection models established by different algorithms were evaluated using Pearson correlation coefficients (r) and root mean square error (RMSE).

The results of the quantitative detection model by the different network structures are shown in Table 2. R_c and RMSEC represent the correlation coefficient and RMSE of the train set, and R_p and RMSEP represent the correlation coefficient and RMSE of the test set. As shown in Table 2, it can be seen that all the deep learning networks were able to achieve a good model performance, and that among them, 1D-SE-Inception V2 performed the best. The R_p of 1D-SE-Inception V2 increased by approximately 2.36% compared to 1D-Inception V1 and the RMSEP of 1D-SE-Inception V2 decreased by approximately 44.91% compared to 1D-Inception V1.

Table 2. Quantitative detection model results of different network structures.

	Rc	RMSEC	Rp	RMSEP
1D-Inception V1	0.9814	0.5715	0.9616	0.6923
1D-Inception V2	0.9966	0.2322	0.9716	0.5500
1D-SE-Inception V1	0.9996	0.0804	0.9737	0.5067
1D-SE-Inception V2	0.9996	0.0772	0.9843	0.3814

A comparison between the predicted and true values in the train set and test set of the water samples of the best detection model is shown in Figure 7. The abscissa in the figure is the sample number and the ordinate is the TOC concentration value. The errors between the predicted values and the true values in both the train and test sets are relatively small. Few samples have significant errors due to the complexity of the real water and the diversity of the water composition. Specifically, the number of samples taken close to the samples with large errors was small, or there may have been confounding factors, such as rainwater and sewage discharge prior to sampling, which resulted in significant differences between the types of organic matter in the water body and traditional water bodies, leading to slightly larger detection errors. The relationship of the predicted and true TOC in the train set is plotted in Figure 8a. The correlation coefficient $r = 0.9996$ and $RMSE = 0.0772$ indicated that the 1D-SE-Inception V2 network almost reduced the whole deviation in the train set.

**Figure 7.** The comparison plots between the predicted and actual concentration of 1D-SE-Inception V2 algorithm on train set (a); and test set (b).

The model trained on the train set was applied to the test set, and the relationship of the predicted and true TOC of test set is plotted in Figure 8b. The Pearson correlation coefficient r statistic of the best deep learning networks model was 0.9843, which gave a measure of the linear relationship between the predicted and true TOC content. The RMSE was 0.3814, which indicated that the predicted TOC concentrations were close to the TOC concentrations measured by the standard method. As shown above, the SE block effectively assigned weights for features extracted from Inception blocks and suppressed useless redundant information. Results indicated that 1D-SE-Inception V2 can effectively extract the features of UV-VIS absorption spectra and establish an inversion relationship between TOC concentration and UV-VIS absorption spectra, driving the RMSE of the best regression model to approach zero.

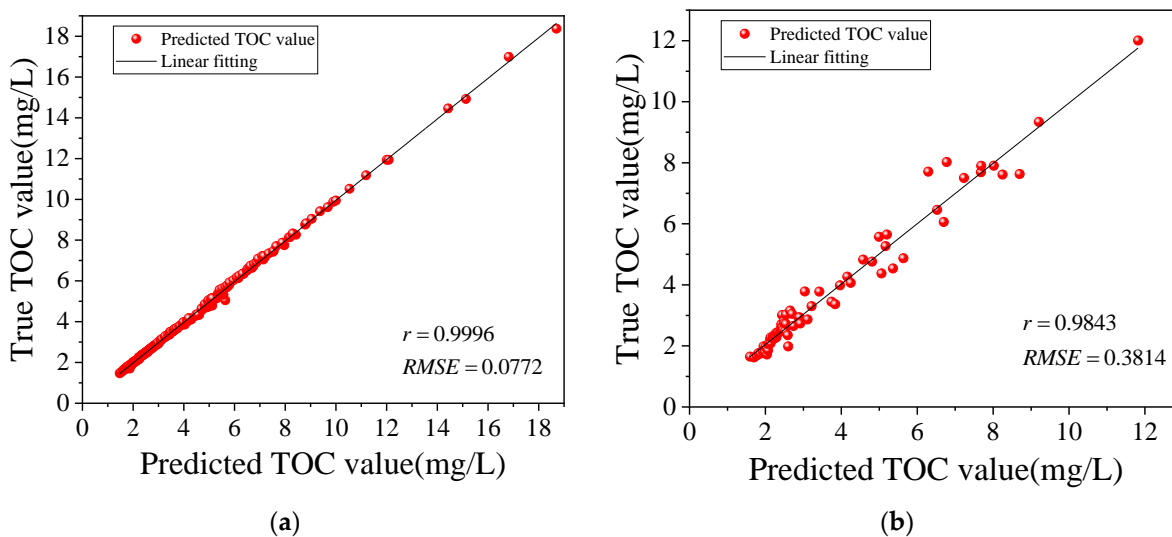


Figure 8. Performance of TOC detection model established by 1D-SE-Inception V2 algorithm on train set (a); and test set (b).

3.3. LSSVM Approach

The LSSVM algorithm is a classical modeling method, which has minimal structural risk and high robustness, and is commonly used in spectral quantitative or qualitative analysis. In this paper, LSSVM was based on the SVM toolkit written by Professor Chih-Jen Lin at National Taiwan University. The best LSSVM model result of train set is shown in Figure 9a. The Pearson correlation coefficient r statistic on the train set is 0.9870 and the RMSE is 0.4059, which means that LSSVM performs well on the train set. The results of the LSSVM prediction of TOC concentrations on the test set are shown in Figure 9b. The Pearson correlation coefficient r statistic on test set is 0.9392, which means that the predicted values and true values are only close to linear. The RMSE on the test set was 0.7723, indicating that the model built by the LSSVM algorithm has a slightly poor fitness on the test set. The reason for this is that the LSSVM has a slightly weaker feature extraction capability compared to deep convolutional networks and may not be able to fully extract a large amount of spectral information from real water samples.

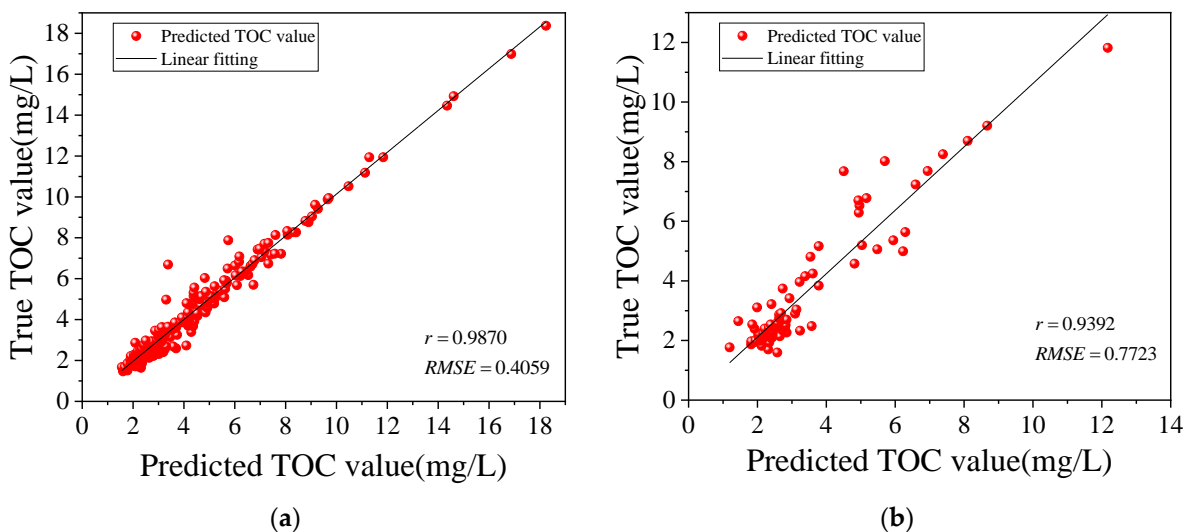


Figure 9. Performance of TOC detection model established by LSSVM algorithm on train set (a); and test set (b).

4. Discussion

The difference between the LSSVM and deep convolutional networks results can be understood not by the considerable amount of UV-VIS spectral information from the complex real water samples, but by the different abilities of the two different methods to utilise complex information for inversion. In general, the advantage of LSSVM lies in the small number of parameters, the rapid training speed, and the ability to train with very small sample sizes. Meanwhile, the feature extraction and modelling capabilities of LSSVM will be relatively poorer in this application scenario than the deep convolutional networks method. Comparing the structures of 1D-Inception V1 and V2, V2 structure replaced the 1×5 convolution with two 1×3 convolutions, which improved the model's ability to express spectral features and thus reducing its prediction error. Comparing the results with, and without, SE modules, Table 2 shows that 1D-Inception V1 and V2 with SE block has significantly improved the r and RMSE. This indicates that the SE block utilizes convolutional spectral features extracted from different channels and assigns different weights to enhance feature information and suppress the interference from useless information.

However, although 1D-SE-Inception V2 can provide a relatively adequate analysis of TOC concentrations in UV-VIS absorption spectra data when applied correctly, it may not be flawless in every region. A small number of special samples from different regions or with different distributions of certain components may have a significant impact on the accuracy of the established model, leading to unsatisfactory prediction results. In practice, these problems are unavoidable, but the impact will be gradually reduced by continuously increasing the number of real samples covering different water components.

5. Conclusions

TOC refers to the total carbon content of suspended or dissolved organic matter in water, which can more comprehensively reflect the total amount of organic pollutants in water. This is also of great importance in the study of the Earth's carbon cycle and climate. Although traditional standard detection methods are accurate, they are time-consuming and labour-intensive. Therefore, it is of great importance to develop a rapid and convenient quantitative detection method for TOC in practical applications. In this study, samples collected from oceans and rivers in several cities in China were analyzed in the laboratory using a UV-VIS absorption spectrometer. The network structure was redesigned to be suitable for one-dimensional spectra, and the inversion relationship between TOC concentration and UV-VIS absorption spectra was established by 1D-Inception V1&V2 and 1D-SE-Inception V1&V2 network structures. Comparing the effects of different structural models, small convolutional kernels improved the ability to express spectral features, and SE blocks allocated weights of different channels to enhance feature information, suppress interference from useless information, and thus reduce prediction errors. The comparison with the LSSVM method further indicated that deep convolutional networks provide better performance in TOC prediction. An optimal detection model was established using 1D-SE-Inception V2, with an $R_c = 0.9996$ and $RMSEC = 0.0772$ in the train set and an $R_p = 0.9843$ and $RMSEP = 0.3814$ in the test set. Rapid and accurate measurements of TOC in water can be achieved by using UV-VIS absorption spectroscopy and deep convolutional networks.

The research results of this paper have important application value in the fields of abnormal water-quality detection, carbon monitoring systems and spectral analysis. On the one hand, researchers can deploy micro-ultraviolet absorption spectrometers on buoys or measure continuously on land. The TOC can be determined with a high degree of temporal resolution and the changes in concentrations over a long period of time can also be observed by means of on-site UV-VIS spectroscopy. The ability to track small timescale changes in TOC is a valuable means of monitoring water-quality anomalies and the ocean's carbon sink and cycle. On the other hand, the 1D-SE-Inception neural network was applied to the detection of TOC and showed good results when the corresponding network structure was modified. The work of this article has significance for the application of the 1D-SE-Inception

model in spectral TOC detection and may both inspire and provide strong support for the application of neural networks in quantitative spectral analysis.

In future work, higher sampling frequencies and more water samples from different regions may improve the predictive accuracy of the detection models. With the help of time series analysis, real-time pollution alerts can be achieved and early warnings for biological disasters, such as red tides, may be provided.

Author Contributions: Conceptualization, W.B. and G.F.; Data curation, X.F.; Formal analysis, Y.L.; Funding acquisition, W.B. and G.F.; Investigation, Y.L., W.B., Y.J. and B.W.; Methodology, Y.L. and Y.J.; Project administration, W.J. and X.F.; Supervision, W.B. and X.F.; Validation, B.W.; Writing—original draft, Y.L. and Y.J.; Writing—review & editing, W.B., W.J., G.F. and X.F. All authors have read and agreed to the published version of the manuscript.

Funding: This research was funded by National Key R&D Program of China [Grant No. 2017YFC1403800]; National Key R&D Program of China [Grant No. 2019YFC1407904]; S&T Program of Hebei [Grant No. 205A3901D].

Data Availability Statement: Data sharing not applicable.

Conflicts of Interest: The authors declare no conflict of interest.

References

1. Yu, J.; Zhou, D.; Yu, M.; Yang, J.; Li, Y.; Guan, B.; Wang, X.; Zhan, C.; Wang, Z.; Qu, F. Environmental Threats Induced Heavy Ecological Burdens on the Coastal Zone of the Bohai Sea, China. *Sci. Total Environ.* **2021**, *765*, 142694. [[CrossRef](#)]
2. Wang, H.; Wang, T.; Xue, G.; Zhao, J.; Ma, W.; Qian, Y.; Wu, M.; Zhang, Z.; Gao, P.; Su, C.; et al. Key Technologies and Equipment for Contaminated Surface/Groundwater Environment in the Rural River Network Area of China: Integrated Remediation. *Environ. Sci. Eur.* **2021**, *33*, 1–16. [[CrossRef](#)]
3. Ma, T.; Zhao, N.; Ni, Y.; Yi, J.; Wilson, J.P.; He, L.; Du, Y.; Pei, T.; Zhou, C.; Song, C.; et al. China's Improving Inland Surface Water Quality since 2003. *Sci. Adv.* **2020**, *6*, eaa03798. [[CrossRef](#)] [[PubMed](#)]
4. Zhou, W.; Zhang, Y.; Yin, J.; Zhou, J.; Wu, Z. Evaluation of Polluted Urban River Water Quality: A Case Study of the Xunsi River Watershed, China. *Environ. Sci. Pollut. Res.* **2022**, *29*, 68035–68050. [[CrossRef](#)] [[PubMed](#)]
5. Han, M.; Liu, F.; Kang, Y.; Zhang, R.; Yu, K.; Wang, Y.; Wang, R. Occurrence, Distribution, Sources, and Bioaccumulation of Polycyclic Aromatic Hydrocarbons (PAHs) in Multi Environmental Media in Estuaries and the Coast of the Beibu Gulf, China: A Health Risk Assessment through Seafood Consumption. *Environ. Sci. Pollut. Res.* **2022**, *29*, 52493–52506. [[CrossRef](#)]
6. Church, M.J.; Ducklow, H.W.; Karl, D.M. Multiyear Increases in Dissolved Organic Matter Inventories at Station ALOHA in the North Pacific Subtropical Gyre. *Limnol. Oceanogr.* **2002**, *47*, 1–10. [[CrossRef](#)]
7. Avril, B. DOC Dynamics in the Northwestern Mediterranean Sea (DYFAMED Site). *Deep-Sea Res. Pt. II* **2002**, *49*, 2163–2182. [[CrossRef](#)]
8. Li, X.; Yu, F.; Cao, J.; Fu, P.; Hua, X.; Chen, Q.; Li, J.; Guan, D.; Tripathee, L.; Chen, Q.; et al. Chromophoric Dissolved Organic Carbon Cycle and Its Molecular Compositions and Optical Properties in Precipitation in the Guanzhong Basin, China. *Sci. Total Environ.* **2022**, *814*, 152775. [[CrossRef](#)]
9. Haywood, B.J.; White, J.R.; Cook, R.L. Investigation of an Early Season River Flood Pulse: Carbon Cycling in a Subtropical Estuary. *Sci. Total Environ.* **2018**, *635*, 867–877. [[CrossRef](#)]
10. Yoon, G.; Park, S.-M.; Yang, H.; Tsang, D.C.W.; Alessi, D.S.; Baek, K. Selection Criteria for Oxidation Method in Total Organic Carbon Measurement. *Chemosphere* **2018**, *199*, 453–458. [[CrossRef](#)]
11. Sharp, J.H.; Benner, R.; Bennett, L.; Carlson, C.A.; Fitzwater, S.E.; Peltzer, E.T.; Tupas, L.M. Analyses of Dissolved Organic Carbon in Seawater: The JGOFS EqPac Methods Comparison. *Mar. Chem.* **1995**, *48*, 91–108. [[CrossRef](#)]
12. Halewood, E.; Opalk, K.; Custals, L.; Carey, M.; Hansell, D.A.; Carlson, C.A. Determination of Dissolved Organic Carbon and Total Dissolved Nitrogen in Seawater Using High Temperature Combustion Analysis. *Front. Mar. Sci.* **2022**, *9*, 1061646. [[CrossRef](#)]
13. Stefánsson, A.; Gunnarsson, I.; Giroud, N. New Methods for the Direct Determination of Dissolved Inorganic, Organic and Total Carbon in Natural Waters by Reagent-FreeTM Ion Chromatography and Inductively Coupled Plasma Atomic Emission Spectrometry. *Anal. Chim. Acta* **2007**, *582*, 69–74. [[CrossRef](#)] [[PubMed](#)]
14. Szabo, H.M.; Tuhkanen, T. The Application of HPLC–SEC for the Simultaneous Characterization of NOM and Nitrate in Well Waters. *Chemosphere* **2010**, *80*, 779–786. [[CrossRef](#)] [[PubMed](#)]
15. Torres, A.; Bond, T.C.; Lehmann, C.M.B.; Subramanian, R.; Hadley, O.L. Measuring Organic Carbon and Black Carbon in Rainwater: Evaluation of Methods. *Aerosol Sci. Tech.* **2014**, *48*, 239–250. [[CrossRef](#)]
16. Etheridge, J.R.; Birgand, F.; Osborne, J.A.; Osburn, C.L.; Burchell, M.R.; Irving, J. Using in Situ Ultraviolet-Visual Spectroscopy to Measure Nitrogen, Carbon, Phosphorus, and Suspended Solids Concentrations at a High Frequency in a Brackish Tidal Marsh: In Situ Spectroscopy to Monitor N, C, P, TSS. *Limnol. Oceanogr. Methods* **2014**, *12*, 10–22. [[CrossRef](#)]

17. Weishaar, J.L.; Aiken, G.R.; Bergamaschi, B.A.; Fram, M.S.; Fujii, R.; Mopper, K. Evaluation of Specific Ultraviolet Absorbance as an Indicator of the Chemical Composition and Reactivity of Dissolved Organic Carbon. *Environ. Sci. Technol.* **2003**, *37*, 4702–4708. [[CrossRef](#)]
18. Spencer, R.G.M.; Butler, K.D.; Aiken, G.R. Dissolved Organic Carbon and Chromophoric Dissolved Organic Matter Properties of Rivers in the USA. *Geophys. Res.* **2012**, *117*, G03001. [[CrossRef](#)]
19. Kim, C.; Ji, T. Real-Time Spectroscopic Methods for Analysis of Organic Compounds in Water. *Curr. Opt. Photonics* **2019**, *3*, 336–341. [[CrossRef](#)]
20. Causse, J.; Thomas, O.; Jung, A.-V.; Thomas, M.-F. Direct DOC and Nitrate Determination in Water Using Dual Pathlength and Second Derivative UV Spectrophotometry. *Water Res.* **2017**, *108*, 312–319. [[CrossRef](#)]
21. Carter, H.T.; Tipping, E.; Koprivnjak, J.-F.; Miller, M.P.; Cookson, B.; Hamilton-Taylor, J. Freshwater DOM Quantity and Quality from a Two-Component Model of UV Absorbance. *Water Res.* **2012**, *46*, 4532–4542. [[CrossRef](#)] [[PubMed](#)]
22. Peacock, M.; Evans, C.D.; Fenner, N.; Freeman, C.; Gough, R.; Jones, T.G.; Lebron, I. UV-Visible Absorbance Spectroscopy as a Proxy for Peatland Dissolved Organic Carbon (DOC) Quantity and Quality: Considerations on Wavelength and Absorbance Degradation. *Environ. Sci.: Process. Impacts* **2014**, *16*, 1445–1461. [[CrossRef](#)] [[PubMed](#)]
23. Wang, G.-S.; Hsieh, S.-T. Monitoring Natural Organic Matter in Water with Scanning Spectrophotometer. *Environ. Int.* **2001**, *26*, 205–212. [[CrossRef](#)]
24. Avagyan, A.; Runkle, B.R.K.; Kutzbach, L. Application of High-Resolution Spectral Absorbance Measurements to Determine Dissolved Organic Carbon Concentration in Remote Areas. *J. Hydrol.* **2014**, *517*, 435–446. [[CrossRef](#)]
25. Dahlén, J.; Karlsson, S.; Bäckström, M.; Hagberg, J.; Pettersson, H. Determination of Nitrate and Other Water Quality Parameters in Groundwater from UV/Vis Spectra Employing Partial Least Squares Regression. *Chemosphere* **2000**, *40*, 71–77. [[CrossRef](#)]
26. Liu, X.; Wang, L. Use of Multivariate Calibration Models Based on UV-Vis Spectra for Seawater Quality Monitoring in Tianjin Bohai Bay, China. *Water Sci. Technol.* **2015**, *71*, 1444–1450. [[CrossRef](#)]
27. Lourenço, N.D.; Menezes, J.C.; Pinheiro, H.M.; Diniz, D. Development of PLS calibration models from UV-Vis spectra for TOC estimation at the outlet of a fuel park wastewater treatment plant. *Environ. Technol.* **2008**, *29*, 891–898. [[CrossRef](#)]
28. Zhang, H.; Zhang, L.; Wang, S.; Zhang, L. Online Water Quality Monitoring Based on UV-Vis Spectrometry and Artificial Neural Networks in a River Confluence near Sheffield-on-Loddon. *Environ. Monit. Assess.* **2022**, *194*, 630. [[CrossRef](#)]
29. Lecun, Y.; Bottou, L.; Bengio, Y.; Haffner, P. Gradient-Based Learning Applied to Document Recognition. *Proc. IEEE* **1998**, *86*, 2278–2324. [[CrossRef](#)]
30. Krizhevsky, A.; Sutskever, I.; Hinton, G.E. ImageNet Classification with Deep Convolutional Neural Networks. In Proceedings of the 25th International Conference on Neural Information Processing Systems, Stateline, NV, USA, 3–6 December 2012. [[CrossRef](#)]
31. Simonyan, K.; Zisserman, A. Very Deep Convolutional Networks for Large-Scale Image Recognition. *arXiv* **2014**. [[CrossRef](#)]
32. He, K.; Zhang, X.; Ren, S.; Sun, J. Deep Residual Learning for Image Recognition. In Proceedings of the 2016 IEEE Conference on Computer Vision and Pattern Recognition (CVPR), Las Vegas, NV, USA, 27–30 June 2016. [[CrossRef](#)]
33. Szegedy, C.; Liu, W.; Jia, Y.; Sermanet, P.; Reed, S.; Anguelov, D.; Erhan, D.; Vanhoucke, V.; Rabinovich, A. Going Deeper with Convolutions. In Proceedings of the 2015 IEEE Conference on Computer Vision and Pattern Recognition (CVPR), Boston, MA, USA, 7–12 June 2015. [[CrossRef](#)]
34. Hu, J.; Shen, L.; Sun, G. Squeeze-and-Excitation Networks. In Proceedings of the 2018 IEEE Conference on Computer Vision and Pattern Recognition (CVPR), Salt Lake City, UT, USA, 18–23 June 2018. [[CrossRef](#)]

Disclaimer/Publisher’s Note: The statements, opinions and data contained in all publications are solely those of the individual author(s) and contributor(s) and not of MDPI and/or the editor(s). MDPI and/or the editor(s) disclaim responsibility for any injury to people or property resulting from any ideas, methods, instructions or products referred to in the content.